Biomaterials 30 (2009) 5114–5124

Contents lists available at ScienceDirect

Biomaterials

journal homepage: www.elsevier.com/locate/biomaterials

Folic acid–Pluronic F127 magnetic nanoparticle clusters for combined targeting, diagnosis, and therapy applications

Jia-Jyun Lin [a], Jenn-Shing Chen [b,**], Shih-Jer Huang [d], Jyun-Han Ko [d], Yu-Ming Wang [c], Ting-Lung Chen [c], Li-Fang Wang [d,*]

[a] Department of Life Science, National University of Kaohsiung, Kaohsiung City 811, Taiwan
[b] Department of Applied Chemistry, National University of Kaohsiung, Kaohsiung City 811, Taiwan
[c] Department of Biological Science and Technology, National Chiao Tung University, Hsinchu 300, Taiwan
[d] Faculty of Medicinal & Applied Chemistry, School of Life Science, Kaohsiung Medical University, Kaohsiung City 80708, Taiwan

ARTICLE INFO

Article history:
Received 1 May 2009
Accepted 4 June 2009
Available online 26 June 2009

Keywords:
Fe_3O_4
Pluronic F127
Folic acid
Magnetic nanoparticles
Diagnosis
Therapy

ABSTRACT

Superparamagnetic iron oxides possess specific magnetic properties in the presence of an external magnetic field, which make them an attractive platform as contrast agents for magnetic resonance imaging (MRI) and as carriers for drug delivery. In this study, we investigate the drug delivery and the MRI properties of folate-mediated water-soluble iron oxide incorporated into micelles. Pluronic® F127 (PF127), which can be self-assembled into micelles upon increasing concentration or raising temperatures, is used to decorate water-soluble polyacrylic acid-bound iron oxides (PAAIO) via a chemical reaction. Next, the hydrophobic dye Nile red is encapsulated into the hydrophobic poly(propylene oxide) compartment of PF127 as a model drug and as a fluorescent agent. Upon encapsulation, PAAIO retains its superparamagnetic characteristics, and thus can be used for MR imaging. A tumor-specific targeting ligand, folic acid (FA), is conjugated onto PF127–PAAIO to produce a multifunctional superparamagnetic iron oxide, FA–PF127–PAAIO. FA–PF127–PAAIO can be simultaneously applied as a diagnostic and therapeutic agent that specifically targets cancer cells that overexpress folate receptors in their cell membranes. PF127–PAAIO is used as a reference group. Based on FTIR and UV–vis absorbance spectra, the successful synthesis of PF127–PAAIO and FA–PF127–PAAIO is realized. The magnetic nanoparticle clusters of PF127–PAAIO and FA–PF127–PAAIO are visualized by transmission electron microscope (TEM). FA–PF127–PAAIO, together with a targeting ligand, displays a higher intracellular uptake into KB cells. This result is confirmed by laser confocal scanning microscopy (CLSM), flow cytometry, and atomic absorption spectroscopy (AAS) studies. The hysteresis curves, generated by using a superconducting quantum interference device (SQUID) magnetometer analysis, demonstrate that the magnetic nanoparticles are superparamagnetic with insignificant hysteresis. The MTT assay explains the negligible cell cytotoxicity of PF127–PAAIO and FA–PF127–PAAIO. In KB cells, the *in vitro* MRI study indicates the better T_2-weighted images in FA–PF127–PAAIO than in PF127–PAAIO.

1. Introduction

Recent advances in nanotechnology have improved the ability to specifically tailor the features and properties of magnetic nanoparticles (MNPs) for diagnosis, therapy, and separation applications [1,2]. Along with the high magnetization values and stable water dispersion, the special surface tailored MNPs not only improve its non-toxic and biocompatibility but also allow the targeting of specific tissues. For this purpose, molecular or macroscopic agents, such as monoclonal antibodies [3,4], peptides [5–7] or small molecules [8,9], are often used to functionalize MNPs to target malignant tumors with high affinity and specificity. Several review articles have been published recently to address the progress of using MNPs for biomedical imaging and therapy applications [10–13]. All these review articles direct us to design MNPs having multifunctional characteristics with complimentary roles. However, one of the major challenges is to provide a surface coating material that can not only prevent biofouling of MNPs in blood plasma, but can also provide active functional groups for controllable conjugation of biomolecules onto

* Correspondence to: Li-Fang Wang, Kaohsiung Medical University, School of Life Science, 100, Shih-Chuan 1st Road, Kaohsiung City 807, Taiwan. Tel.: +886 7 3121101x2217; fax: +886 7 3125339.
** Corresponding author. Tel.: +886 7 5919463; fax: +886 7 5919348.
E-mail addresses: jschen@nuk.edu.tw (J.-S. Chen), lfwang@kmu.edu.tw (L.-F. Wang).

0142-9612/$ – see front matter © 2009 Elsevier Ltd. All rights reserved.
doi:10.1016/j.biomaterials.2009.06.004

MNPs to induce a specific targeting property. A common method to prevent the biofouling by proteins is to PEGlyate the MNPs on the surface [14–16]. PEGylation of MNPs also confers several important properties such as high solubility and stability in aqueous solutions, biocompatibility, and prolonged blood circulation time. In addition to PEGlyation, dextran has often been used to coat the surface of MNPs [17,18]. The dextran-coated MNPs can often be easily detached from the surface of MNPs due to the weak interaction between MNPs and dextran. This detachment leads to aggregation and precipitation under physiological conditions [19].

We synthesized a highly water-soluble Fe_3O_4 via a one-step hydrolysis reaction of $FeCl_3$ at high temperature in the presence of a low molecular weight capping agent, polyacrylic acid (PAA). We chose Pluronic F127 (PF127) to decorate MNPs because it is a copolymer consisting poly(ethylene oxide)–poly(propylene oxide)–poly(ethylene oxide) blocks, PEO_{100}–PPO_{65}–PEO_{100}. The exterior PEO corona provides an antifouling character to prevent aggregation, protein adsorption, and recognition by the reticuloendothelial system (RES) [20] and the hydrophobic PPO core can be adapted to encapsulate the hydrophobic anticancer agents or fluorophores. The self-assembling characteristics of PF127 at either raising temperatures or increasing concentrations have been extensively explored for controlled drug delivery applications especially in the form of micelles [21–23]. The carboxylic acid groups of PAAIO were used to chemically conjugate the hydroxyl groups of PF127 to form the stable PF127-decorated MNPs. When using dextran- or PEG-coated iron oxide particle as MNPs for drug delivery systems, the drug of interest can be only conjugated with limited functional sites of the coated dextran [17] or PEG [9,24], while PF127, the drug can be loaded either by chemical conjugation or by physical encapsulation due to its self-assembly characteristics.

An oleic acid-coated iron oxide and PF127 stabilized MNPs have been developed for drug delivery of doxorubicin and/or paclitaxel for MRI [23]. Recently, Dexamethasone (DXM), was encapsulated into PLGA coated MNPs for the local treatment of arthritis [25,26]. Both polymer-coated MNPs have been applied as a drug delivery carrier as well as a diagnostic imaging agent, but lack a targeting moiety to direct the polymer-coated MNPs specifically to tumor tissues. Peng et al. [12] have recently reviewed the advantages and limitations of using various types of ligands modified on MNPs. The tumor-targeted MNPs were categorized for tumor imaging and selective drug delivery vehicles, and it seems apparent that very few studies have used targeted MNPs for simultaneous drug delivery and diagnostic imaging. Indeed, Nasongkla and colleagues [27] have developed multifunctional polymeric micelles with cancer-targeting capabilities via $\alpha_v\beta_3$ integrins, controlled drug delivery, and MRI contrast characteristics. By a solvent-evaporation method, the loading efficiencies of 6.7 and 2.7 wt% of hydrophobic iron oxides and DOX were physically loaded into the amphiphilic block copolymers. cRGD was covalently attached to the micellar surface through a thiol–maleimide linkage. The DOX loaded MNPs with cRGD showed improved internalization into SLK cells compared to without. A similar system was developed that utilizes a multifunctional magneto-polymeric hybrid nanosystems (MMPNs). This system was generated by loading 41.7 wt% of $MnFe_2O_4$ and 40.9 wt% Fe_3O_4 magnetic iron oxides inside micelles [28]. An anti-HER antibody (HER, Herceptin) was conjugated to the MMPNs surface by utilizing the carboxyl group on the surface of the MMPNs. The HER-conjugated MMPNs showed significant targeting efficiency to HER2/neu receptors overexpressed in NIH3T6.7 cells. In addition, the synergetic effect on inhibition of tumor growth was observed when combined with DOX.

The low molecular weight of folic acid (FA, $F_w = 441.4$ g/mol, vitamin B9) binds selectively to folate receptor (FR), a glycosylphosphaidylinositol-anchored cell surface receptor overexpressed in many human tumors [29,30]. These nutrient pathways are attractive since they are directly related to cell proliferation. The most aggressive tumor cells will cause an increase in cellular uptake in the presence of particles having the FA moiety. Sega and Low summarized six advantages using FRs as targets for molecular imaging [31]. In this study, we developed a novel multifunctional MNP. Instead of dispersing iron oxide particles in micelles, the chemical reaction between the iron oxide particles and PF127 was prepared. FA–PF127–PAAIO having simultaneously targeting FA, can be used for MRI diagnosis, and can be used for chemical therapy. The summarized merits of our synthesized MNP will include (1) the carboxylate groups on PAA strongly coordinate to iron cations on Fe_3O_4 surface, and the uncoordinated carboxylate groups extend into the aqueous phase (as shown by the high degree of dispersion in water) and permits further chemical reaction with PF127, (2) the PPO segments of PF127 provide a hydrophobic environment to encapsulate hydrophobic agents for drug delivery or for fluorescent imaging, and the hydrophilic corona prevents RES recognition, and (3) FA conjugated onto PF127-bound MNPs meets most of the promising characteristics for folate receptors as tumor targeting agents. The synthesized MNPs were analyzed by FTIR and UV–vis spectrophotometers. The physical properties and performance of the MNPs were characterized by dynamic light scattering (DLS), TEM, AAS, flow cytometry, SQUID and MR imaging. The dual imaging of Nile red and MNP clusters internalized into KB cells was accomplished by CLSM.

2. Materials and methods

2.1. Materials

Folic acid, iron(III) chloride anhydrous ($FeCl_3$, F_w 162.21 g/mol), and sodium hydroxide were acquired from TCI (Tokyo, Japan). Pluronic F127 was purchased from Aldrich (St. Louis, USA). 1,1′-Carbonyldiimidazole (CDI) and poly(acrylic acid) (PAA, Mw = 2000) were obtained from Acros (New Jersey, USA). Fetal bovine serum (FBS) was purchased from Biological Industries (Beit Haemek, Israel). RPMI 1640 and trypsin-EDTA were obtained from Invitrogen (Carlsbad, CA, USA). 3-(4,5-Dimethylthiazol-2yl)-2,5-diphenyl tetrazolium bromide (MTT) and Nile red were acquired from MP Biomedicals (Eschwege, Germany). All other unstated chemicals were obtained from Sigma Chemical Company (St. Louis, USA), and used without further purification.

2.2. Synthesis of Pluronic F127–folic acid adduct (FA–PF127)

87.58 mg (0.20 mmol) of FA was dissolved in 3 mL of dried DMSO and added to a one neck flask. Next, 35.32 mg (0.22 mmol) CDI was added, and the reaction was stirred for one day at rt in the dark. 0.62 g (0.05 mmol) of PF127 which has been previously dried overnight in vacuum, was added to the above solution. The reaction was allowed to proceed in the dark for 1 d at rt. The reaction mixture was transferred into a dialysis tube (Spectra, Millipore, MWCO 1000) and dialyzed for 3 d against double deionized (DD) water, which was changed every 3–6 h. FA–PF127 was recovered via lyophilization. The resulting product was dried in a vacuum oven for 2 d, yielding ~51% of product. The product was stored in a dry box until use.

2.3. Synthesis of poly(acrylic acid)-bound iron oxide (PAAIO), PF127–PAAIO and FA–PF127–PAAIO

A one-step synthesis for highly water-soluble magnetite (Fe_3O_4) nanocrystals with PAA-bound on the surface was done according to the literature [32] with slight modification. In general, the synthesis proceeded as follows. A sodium hydroxide/diethylene glycol (NaOH/DEG) stock solution was prepared by dissolving 50 mmol of NaOH in 20 mL DEG. This solution was heated to 120 °C for 1 h under nitrogen, and was then cooled and kept at 70 °C. A mixture of PAA (0.63 g, 0.32 mmol), and $FeCl_3$ (1.50 g, 9.25 mmol) in 75 mL DEG was heated to 220 °C in a nitrogen atmosphere for 30 min under vigorous stirring. Next, 20 mL of the NaOH/DEG stock solution was rapidly injected into the above reaction solution. The resulting solution was further reacted for 10 min. The product was repeatedly purified by precipitation using DD water as a solvent and 95% ethanol as a non-solvent. Then the precipitate was redissolved in 50 mL DD water and filtered using a 0.2 μm filter. The black solid product was obtained via lyophilization and kept at −20 °C for further use.

PF127–PAAIO and FA–PF127–PAAIO were synthesized via *N*-(3-dimethyl aminopropyl)-3-ethylcarbodiimide hydrochloride (EDAC) mediated ester formation. Briefly, 40 mg of EDAC was added to a solution of 20 mg of PAAIO dissolved in 20 mL of DD water. The reaction was adjusted to pH = 7.0 and stirred for 1 d at rt. Next,

20 mg of PF127 or FA–PF127 was added into the above solution and the reaction was carried out in the dark for 2 d at rt. The solution was poured into a dialysis membrane (MWCO 25000) and dialyzed against DD water, which was changed every 3–6 h for 2 d. The aqueous solutions were freeze-dried and the resulting products were stored at −20 °C for further use.

2.4. Nile red encapsulation

Nile red was used as a fluorescence probe as well as a model hydrophobic agent. Five mg of PF127–PAAIO or FA–PF127–PAAIO was dissolved in 5 mL of DD water and 150 μL of Nile red at a concentration 0.34 mg/mL in DMSO was slowly transferred via pipette into the above solution and stirred in darkness for 1 d. The solution was lyophilized to remove DMSO. The remaining solid was redispersed into 5 mL of DD water followed by filtration using a 0.45 μm filter to remove free Nile red. The solution was freeze-dried and the Nile red-encapsulated MNPs were stored under light protection at −20 °C for further use.

2.5. Characterizations

^{1}H-NMR spectrum of FA–PF127 was recorded on a Gemini-200 spectrometer (Varian, CA, USA) using deuterium dimethyloxide (DMSO-d_6) as a solvent. The qualitative proof of folic acid groups on PAAIO surface was carried out by UV–visible spectrophotometer (Agilent 8453, CA, USA). The absorbance wavelength was set in the range from 200 to 500 nm. The ester bond formation between PAAIO and PF127 (or FA–PF127) was confirmed by Fourier transform infrared (FTIR). FTIR spectra were obtained on a Perkin-Elmer-2000 spectrometer. Dried samples were pressed with KBr powder into pellets. Sixty-four scans were signal-averaged in the range from 4000 to 400 cm^{-1} at a resolution of 4 cm^{-1}.

Particle sizes of MNPs were measured using a Zetasizer Nano S dynamic light scattering (Malvern, Worcestershire, UK). Light scattering measurements were carried out with a laser of wavelength 633 nm at a 90° scattering angle. The concentration of the sample was 0.1 mg/mL and temperature was maintained at 25 °C. CONTIN algorithms were used in the Laplace inversion of the autocorrelation function to obtain size distribution. The mean diameter was evaluated from the Stokes–Einstein equation [33]. The particle diameter and morphology of MNPs were also visualized by cryo-TEM (Jeol JEM-1400, Tokyo, Japan). A carbon coated 200 mesh copper specimen grid (Agar Scientific Ltd. Essex, UK) was glow-discharged for 1.5 min. One drop of the sample solution was deposited on the grid and left to stand for 2 min. After 2 min, excess fluid was removed with a filter paper. The grids were allowed to air-dry at rt and then examined with an electron microscope. X-ray diffraction spectroscopy (XRD) measurements were performed on a Rigako 2 KW spectrometer (Tokyo, Japan) with the following operation conditions: 40 kV and 30 mA with a Cu Kα1 radiation at λ 1.54184 Å. The relative intensity was recorded in the scattering range from 25 to 65° at a rate of $2\theta = 5°$/min. The magnetic properties were measured with a magnetic properties measurement system (MPMS) from Quantum Design (MPMS-XL 7), which utilizes a superconducting quantum interference device (SQUID) magnetometer at fields ranging from −15 to 15 K Oe at 25 °C. The iron concentrations in PAAIO, PF127–PAAIO, and FA–PF127–PAAIO were determined using an atomic absorption spectrophotometer (AAS) positioned at 248 nm (5100 PC, Perkin Elmer, USA).

2.6. Cell culture, cytotoxicity, and cellular uptake

KB cells, an oral epidermoid cell line, obtained from Dr. Cheng's group at Kaohsiung Medical University of Taiwan, were grown and maintained in RPMI 1640 medium. Each cell culture medium was supplemented with 10% inactivated fetal bovine serum (FBS), 100 μg/mL streptomycine, and 100 U/mL penicillin at 37 °C under 5% CO_2.

2.6.1. Cytotoxicity

KB cells were seeded in 96-well tissue culture plates at a density of 5×10^3 cells per well in RPMI 1640 medium containing 10% FBS. After 24 h, the culture medium was replaced with 100 μL of medium containing 5–1000 μg/mL of MNPs. The cytotoxicity was evaluated by determining the viability of the macrophages after incubation for 24 h. The number of viable cells was determined by the estimation of their mitochondrial reductase activity using the tetrazolium-based colorimetric method (MTT conversion test) [34].

2.6.2. Flow cytometry

KB cells (3×10^5) were pre-grown in 6-well culture plates using folic acid-deficient RPMI 1640 medium for 24 h. Next, the Nile red-loaded PF127–PAAIO or FA–PF127–PAAIO was added at a concentration of 50 μg/mL in the same medium and incubated separately for 1 h and 3 h. Next, the culture medium was aspirated and the cells were washed three times with 2 mL of PBS containing 2% FBS. The cells were detached by 1X trypsin and centrifuged at 1200 rpm for 5 min. The media was then removed by aspiration. The cells were resuspended in 2 mL of PBS and 1×10^4 cell accounts were immediately analyzed using a flow cytometer (Beckman Coulter, California, USA). The cellular uptake of MNPs was quantified by AAS, where 2×10^4 cell counts from each sample were analyzed for iron content. The centrifuged cell pellets were dissolved in 37% HCl at 70 °C and let sit for 1 h. The AAS samples were diluted to a volume of 3 mL for analysis. The iron contents of the samples were calculated based on a calibration curve of $FeCl_3$.

2.6.3. Confocal

KB cells (2×10^5 cells in 2 mL PBS) were seeded into a 12-well culture plate in folic acid-deficient RPMI 1640 containing one glass coverslip/well and incubated for 24 h. Next, the medium was removed and 2 mL of folic acid-deficient RPMI 1640 containing Nile red-loaded PF127–PAAIO or FA–PF127–PAAIO at a concentration of 50 or 500 μg/mL was added into each well and incubated at 37 °C for various time periods. The coverslips with cells were then placed in empty wells, treated with 1 mL of 3.7% formaldehyde in PBS, and allowed to sit at rt for 30 min. After three PBS washings, the cells were treated with 1 mL/well of Triton X-100 and incubated for 10 min. Next, the cells were washed three times with PBS and then incubated at 37 °C with 0.5 mL/well of DAPI for 10 min. The cells were analyzed using an Olympus Fv 500 CLSM (Tokyo, Japan). The emission wavelength was set at 568 nm for Nile red. The images were superimposed using the imaging software to observe co-localization.

2.7. In vitro MRI

T_2-weighted signal intensities were measured with a clinical 3.0 T magnetic resonance scanner (Sigma, GE Medical System, Milwaukee, WI, USA) using iron concentrations ranging from 0 to 40 μg/mL in folic acid-deficient RPMI 1640. KB cells (5×10^5 cells) were seeded into a 6-well culture plate 1 d before adding the various concentrations of FA–PF127–PAAIO or PF127–PAAIO. The addition was followed by incubation at 37 °C for 3 h. The media was dispensed and the cells were washed three times with PBS containing 2% FBS. The T_2-weighed images were acquired using a fast gradient echo pulse sequence (TR/TE/flip angle 3000/90/10).

3. Results and discussion

3.1. Synthesis and characterization of MNPs

FA–PF127 was synthesized using the various molar ratios of FA to PF127 to ensure that at least one or more of the two hydroxyl

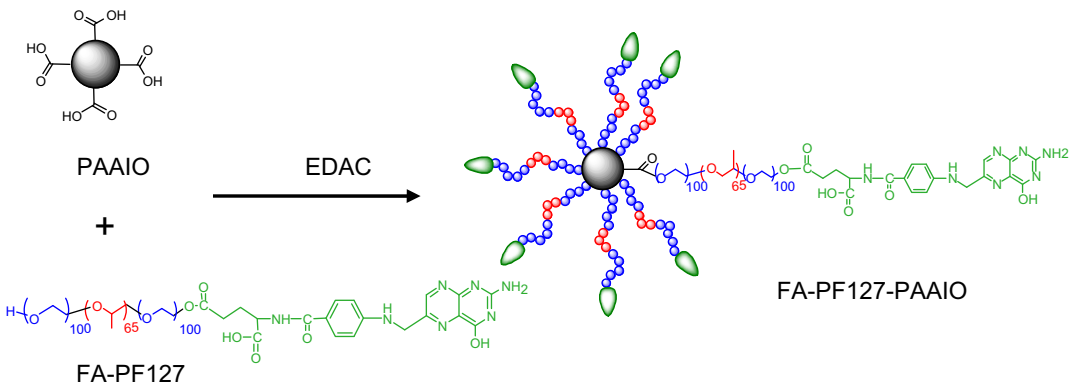

Scheme 1. Schematic illustration of chemical formation of FA–PF127–PAAIO.

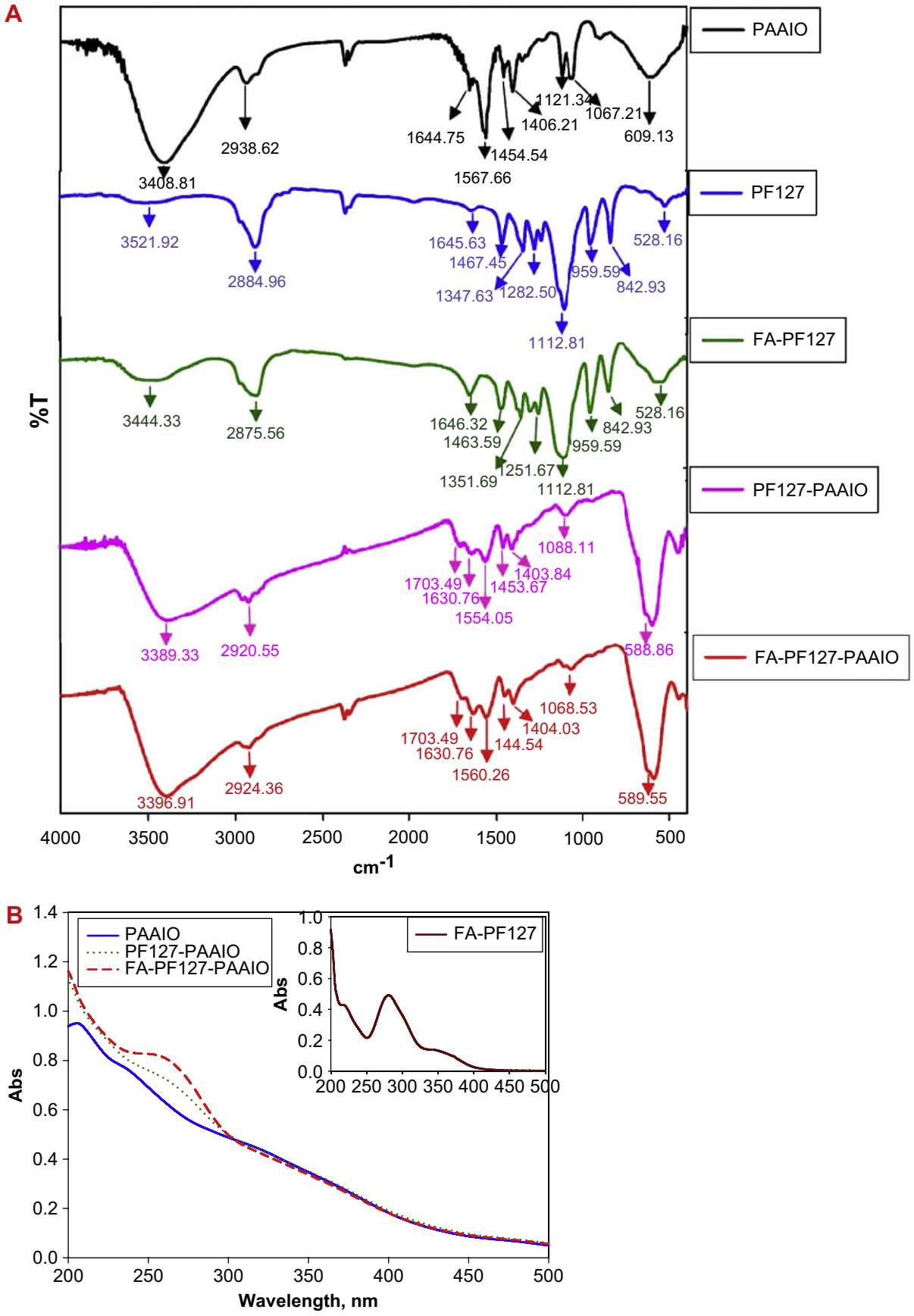

Fig. 1. FTIR spectra of PAAIO, PF127, FA–PF127, PF127–PAAIO, and FA–PF127–PAAIO (A), UV–vis spectra of PAAIO, PF127–PAAIO, FA–PF127–PAAIO, and FA–PF127 (B).

groups of PF127 were conjugated with the carboxylic acid groups of FA. The optimum conditions were determined using NMR, where an optimum molar ratio between PF127 and FA was found to lie at the ratio of 1–4 for 1 d. After dialysis against DD water using a molecular weight cut-off 1000 dialysis membrane, the freeze-dried product was further washed three times with an excess amount of acetone. The final product was dried in a vacuum oven. The NMR spectrum in DMSO-d_6 (Supporting information S1), shows a broad peak at 3.5 ppm (attributed to PEO) and peak that are characteristic of methyl groups on PPO appears at 1.1 ppm. FA signals appear at 6.6 and 7.6 ppm (aromatic protons), and 8.5 ppm (pteridine proton) and the total intensities of these five proton peaks and that of the methyl groups of PPO were measured to calculate the degree of FA substitution onto PF127, which was determined to be ~130 mol%.

A water-soluble PAAIO was synthesized via a one-pot reaction according to the literature [32]. The high temperature hydrolysis of Fe^{3+} upon addition of NaOH/DEG in the presence of low molecular weight PAA (2000 g/mol) yielded highly water-soluble Fe_3O_4. However, the iron oxide particles coagulated when using a high molecular weight of PAA (~140 K g/mol). The PAA-bound iron oxide (PAAIO) retained the characteristic X-ray diffraction pattern of Fe_3O_4 at 2θ of 30.2, 35.5, 43.2, 53.3, 57.1, and 62.8° as listed in ASTM XRD standard card (19-0629) with the reduced signal intensities (Supporting information S2).

As shown in Scheme 1, a conjugation reaction between the hydroxyl groups of PF127 or FA–PF127 and the carboxylic groups of PAAIO was carried out at weight ratio of 1 in aqueous solution at pH = 7.0. Fig. 1A clearly demonstrates the successful chemical conjugation since a characteristic peak of the ester bond stretching appears at 1703 cm^{-1} in PF127–PAAIO and FA–PF127–PAAIO. The other characteristic IR absorbance peaks for carboxylate COO^- of PAAIO displaying at 1567 and 1406 cm^{-1} corresponding to the asymmetric C–O stretching mode and symmetric C–O stretching mode were also observed [32]. A broad peak at 3408 cm^{-1} suggests chemisorption of PAA onto iron oxides. The absorbance IR peak of Fe–O assigned at 609 cm^{-1} [8] could be seen in PAAIO but was replaced by 589 cm^{-1} peak in PF127–PAAIO and FA–PF127–PAAIO. The FTIR technique is insufficient to distinguish FA signals in FA–PF127–PAAIO from those in PF127–PAAIO. Thus a UV–vis spectrum was measured to qualitatively and/or quantitatively measure the content of FA decorated on MNPs. As can be seen in Fig. 1B, a profound UV absorbance peak around 270 nm attributed to the aromatic ring occurs in FA–PF127–PAAIO. Nevertheless, due to the strong background intensity of PAAIO, it is difficult perform a quantitative calculation of FA content from this UV–vis spectrum.

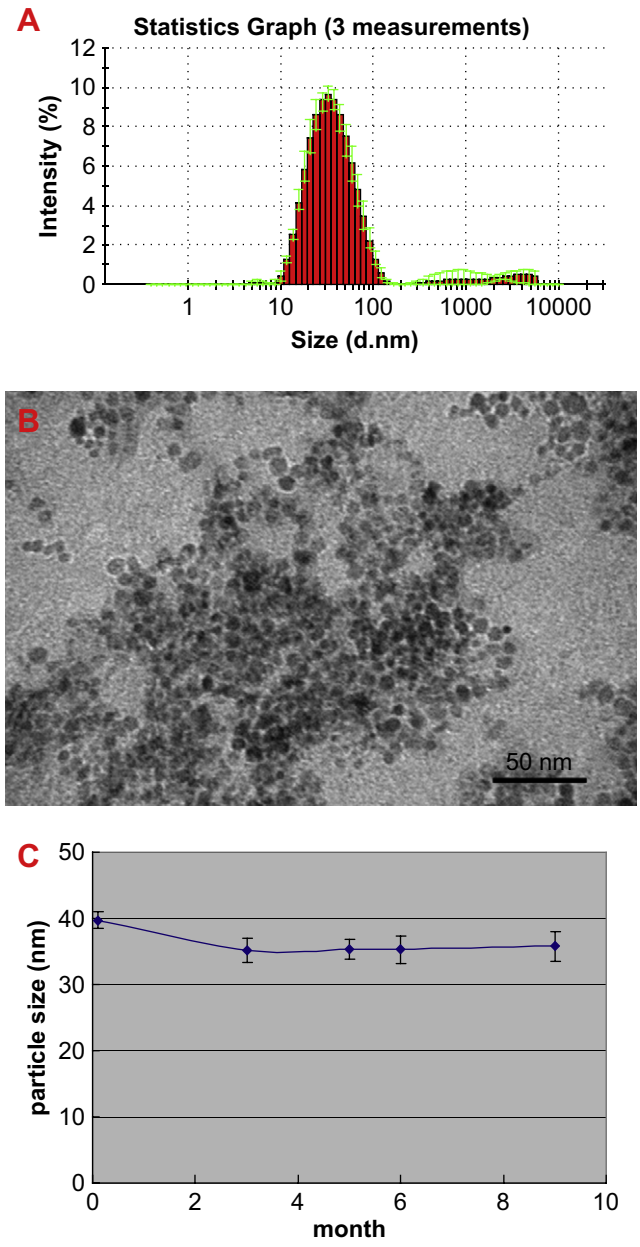

Fig. 2. DLS particle distribution of PAAIO in DD water (A), TEM image of PAAIO (B), PAAIO mean particle diameter change with time (C).

3.2. Particle sizes and zeta potentials of MNPs

The average hydrodynamic diameter measured by DLS for PAAIO in DD water at 0.1 mg/mL without any filtration is shown in Fig. 2A. The DLS result shows the average hydrodynamic diameter of PAAIO is 39.4 ± 2.0 nm (PDI = 0.29) while the particle diameter reduces to 12.0 ± 0.7 nm by cryo-TEM as seen in Fig. 2B. The discrepancy of particle size measured by DLS and by TEM is frequently observed when a hydrophilic polymer layer is coated on a nanoparticle surface. This coating causes an increase in the average hydrodynamic diameter during DLS measurements [35,36]. PAAIO has also been synthesized by Ma and colleagues [37] via a two-step method. Fe_3O_4 was synthesized by reacting $FeCl_3 \cdot 6H_2O$ and $FeCl_2 \cdot 4H_2O$ first and the purified Fe_3O_4 was further reacted with PAA oligomer to form PAAIO. Their PAAIO diameter was 9.6 ± 2.6 nm measured by TEM and was 246 ± 11 nm by DLS. The bigger size discrepancy was reported. Our synthesized PAAIO is stable in DD water for a period of 9 months, and PAAIO is neither aggregated or significantly change in particle diameter (Fig. 2C). Such stability is desirable for use in biological applications. PAAIO was further conjugated with PF127 or FA–PF127 and the particle diameters increase to 113.3 ± 1.2 nm (PDI = 0.21) and 125.4 ± 2.0 nm (PDI = 0.22), respectively as measured by DLS (Supporting information S3). The particle diameters do not significantly change after Nile red was loaded (123.5 ± 2.1 nm, PDI = 0.22 for PF127–PAAIO and 112.3 ± 4.4 nm, PDI = 0.26 for FA–PF127–PAAIO). The zeta potential is −20.7 ± 2.0 mV for PAAIO and turns to −16.6 ± 1.1 nm and −14.7 ± 0.5 nm when PAAIO was shielded with PF127 and FA–PF127. After Nile red was loaded, the zeta potentials are −16.7 ± 1.9 mV and −13.6 ± 1.1 mV.

The TEM morphological images of PF127–PAAIO and FA–PF127–PAAIO with or without Nile red are represented in Fig. 3.

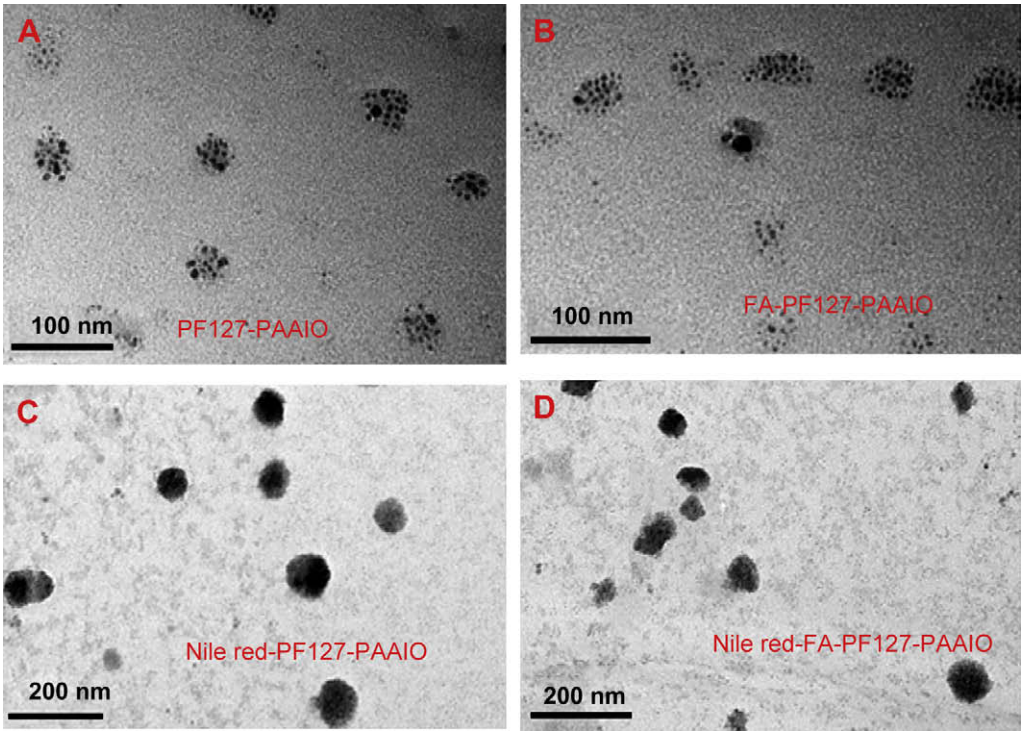

Fig. 3. TEM images of PF127–PAAIO (A), FA–PF127–PAAIO (B) Nile red-loaded PF127–PAAIO (C), and Nile red-loaded FA–PF127–PAAIO (D).

The particle diameters for PF127–PAAIO and FA–PF127–PAAIO, averaged from 30 particles, are 41.3 ± 4.1 and 36.7 ± 9.1 nm respectively. The diameter increases to 80.0 ± 18.8 for PF127–PAAIO and increases to 65.6 ± 16.0 nm FA–PF127–PAAIO when Nile red was loaded. The isolated clusters of magnetic nanoparticles are clearly observed in the PF127–PAAIO or FA–PF127–PAAIO self-assembled micelles, but images of each MNP becomes ambiguous when Nile red was incorporated. This may be due to the fact that Nile red attenuates TEM electron beams. Jain et al. [23] have recently reported a similar formulation of MNPs in which the Fe_3O_4 core was first coated with oleic acid (OA) and then OA-coated iron oxide was stabilized with PF127 to form a water dispersible system. The mean hydrodynamic diameters measured in DD water with or without doxorubicin (DOX) and/or paclitaxel loaded were in the range of 210–250 nm. The result implies that the water-soluble PAA-bound Fe_3O_4 and the chemical conjugation on PAA-bound Fe_3O_4 surface with Pluronic polymers provide smaller and more stable MNPs. Indeed, carboxylates coordinating to the surfaces of MNPs has been investigated [38]. A PEI-modified Pluronic P123 was decorated on a citrated iron oxide complex through strong electrostatic interactions, where also showed a similar particle diameter ($\sim$ 40 nm) by TEM. In the design of a drug delivery carrier, a particle diameter of less than 100 nm is beneficial for MNPs to pass through the cell membranes.

3.3. Composition and SQUID of MNPs

The iron content in PAAIO, PF127–PAAIO, and FA–PF127–PAAIO was determined by AAS, and the values are 37.37 ± 0.02, 13.62 ± 0.06, and 11.22 ± 0.04 wt%, respectively. Given that the weight ratio between the iron and the non-iron portion of PAAIO is taken as 0.59_7 (the ratio between 37.37 and 62.63) then the wt% content of PF127 in PF127–PAAIO is calculated by subtraction of 100 from the wt% content of the iron (13.62 wt%) and the non-iron (22.83 wt%) of PAAIO. The 63.55 wt% content of PF127 is obtained in PF127–PAAIO. Based on the same calculation, the wt% content of FA–PF127 is 69.98 wt% in FA–PF127–PAAIO. The initial wt% of polymer used in the feed was controlled at 50-wt%. The higher contents of polymers obtained imply that the polymer unbound PAAIO could be removed during dialysis and PAAIO is successfully decorated by PF127 or FA–PF127.

For the clinical application as targeted contrast agents for MRI, it is critical that MNPs retain their favorable magnetic properties after

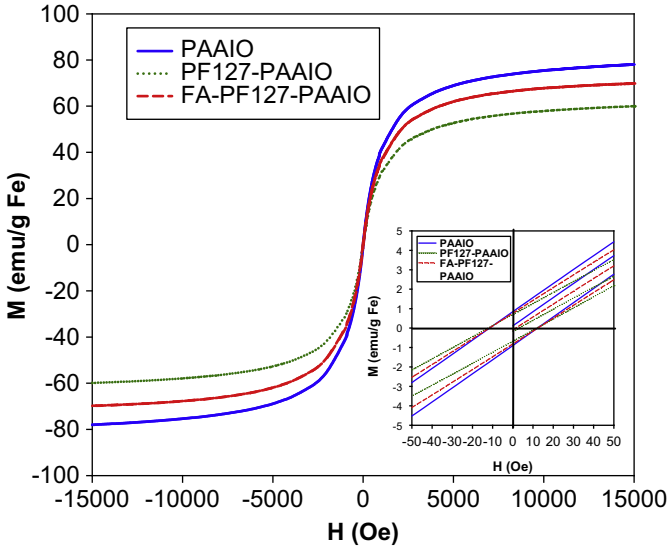

Fig. 4. Magnetization curve as a function of field for MNPs at a temperature of 25 °C. Inset shows the data around zero field with an expanded scale demonstrating that the MPNs are superparamagnetic without hysteresis.

coating with polymers. The magnetic properties of MNPs were investigated with a SQUID magnetometer. The saturation magnetization value of PAAIO, PF127–PAAIO, and FA–PF127–PAAIO was 78.1, 60.0, and 69.8 emu/g Fe at 25 °C (Fig. 4) when normalized using the iron mass (as determined by AAS). As expected, the MNPs are superparamagnetic at rt. The hysteresis loops show negligible hysteresis and the loss of saturation magnetization after the Pluronic polymer coating is insignificant.

3.4. Cytotoxicity and cellular uptake of MNPs

In order to examine the acute toxicity of Pluronic-coated PAAIO with or without Nile red, KB cells were incubated 24 h with MNPs in the concentrations ranging from 5 to 1000 μg/mL. The cell viability, as determined by MTT assay, demonstrates that KB cells incubated with PF127–PAAIO or FA–PF127–PAAIO are non-toxic at all tested concentrations, since the cell growth rates with MNPs are the same as that of the medium control. Conversely, as shown in Fig. 5, the cell viability decreases profoundly when MNPs were loaded with Nile red, where both Nile red-loaded MNPs show ~80% viable cells but independent of the increase in increasing concentrations.

The flow cytometry analysis was used to study the cellular uptake efficacy of MNPs with or without folic acid moiety in FR-positive KB cells. Fig. 6A shows a negligible fluorescent shift relative to the controlled group in the Nile red-loaded PF127–PAAIO, while a distinguishable right shift is observed in the Nile red-loaded FA–PF127–PAAIO, indicating a better cellular uptake even at a low NP concentration of 50 μg/mL at 1 h of incubation. The improved cellular uptake into KB cells of MNPs with a folic acid moiety is increased 10 fold compared to PF127–PAAIO when extending the incubation time period to 3 h (Fig. 6B). For the sake of comparison, a FR deficient cell line, A549, was chosen as a negative control. As seen in Fig. 6C, both PF127–PAAIO and FA–PF127–PAAIO show a low degree of cellular internalization of MNPs into A549 cells after 3 h of incubation at a concentration of 50 μg/mL. This result explains that FA–PF127–PAAIO has the ability to transport folate-linked cargos into FR overexpressed KB cells through a process called receptor-mediated endocytosis [39]. The cellular uptake of MNPs was quantified by measuring the iron content per cell using AAS. The measurement was performed after dissolving the cells in 37% HCl at 70 °C. The mean data of the cellular iron contents in KB cells are 6.1 and

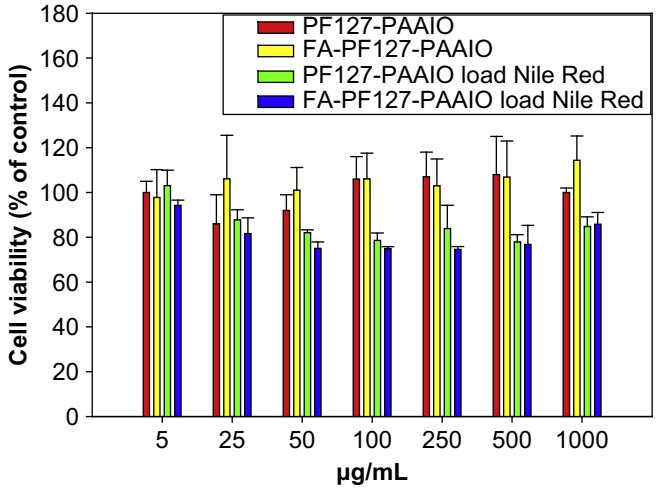

Fig. 5. Cell viability of MNPs in KB cells at the various concentrations.

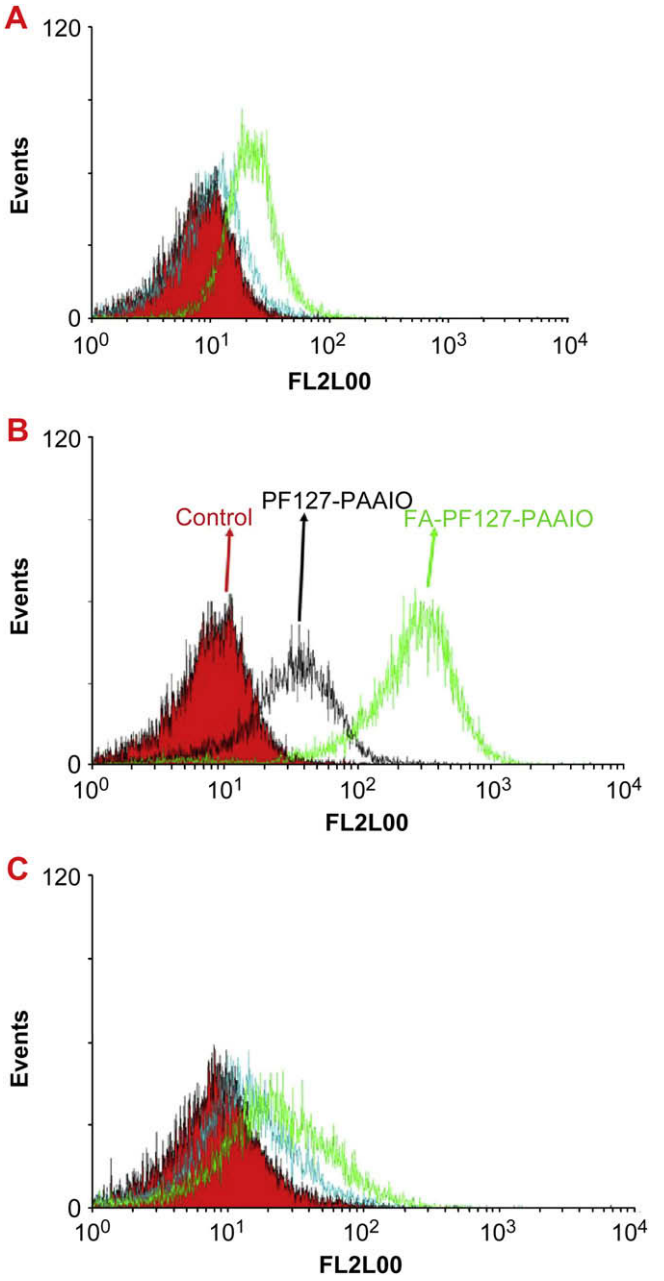

Fig. 6. Flow cytometry histograms of MNPs at a concentration of 50 μg/ml internalized into KB cells for 1 h (A), for 3 h (B), and MNPs internalized into low FR expression A549 cells for 3 h (C).

49.0 pg Fe/cell for PF127–PAAIO and FA–PF127–PAAIO at 1 h of incubation, and 59.7 and 157.5 pg Fe/cell after 3 h of incubation (Fig. 7). This result is in a good agreement with the findings by flow cytometry, where FA–PF127–PAAIO clearly had the better cellular internalization into KB cells. In A549 cells that express low FA receptors, the mean value of the iron contents is lower at 3 h of incubation as compared to KB cells (4.0 pg Fe/cell for FP127–PAAIO and 30.0 pg Fe/cell for FA–PF127–PAAIO).

The cellular uptake image of Pluronic modified MNPs into KB cells was directly visualized by CLSM (Fig. 8), using the same experimental conditions as above. The confocal images of the Nile red-loaded FA–PF127–PAAIO, when compared to the Nile red-loaded PF127–PAAIO, show similar fluorescence intensities at the first hour of incubation and become higher after 3 h of incubation.

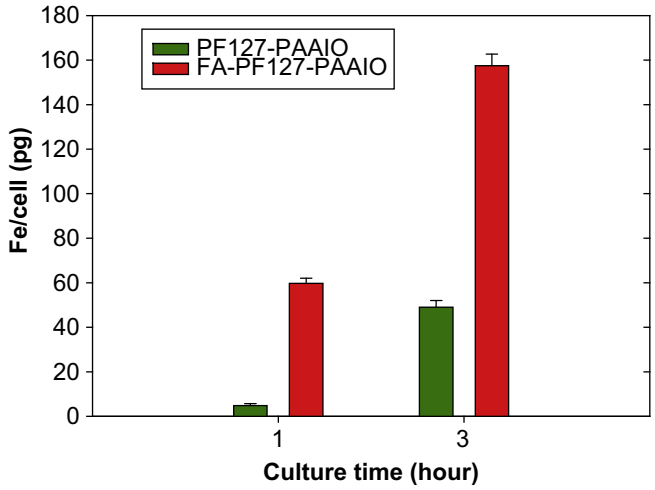

Fig. 7. The iron content in KB cells due to the uptake of PF127–PAAIO and FA–PF127–PAAIO.

The red fluorescence is seen better localized in the nucleus of KB cells in the Nile red-loaded FA–PF127–PAAIO at 3 h, indicating that it is potential to deliver a hydrophobic anticancer agent in the future study. The enhancement of cellular uptake with FA–PF127–PAAIO over PF127–PAAIO goes hand-in-hand with the flow cytometry results. In order to better visualize the MNP clusters inside KB cells, we increased the incubating concentration of MNPs to 500 μg/mL and traced various incubation periods up to 24 h. As can be seen in Fig. 9, the MNP clusters co-localized with Nile red in the cytoplasm are seen in the Nile red-loaded FA–PF127–PAAIO at 1 h of incubation and become clearer when the incubation time increases (see the arrow indexes at 3 h). In contrast the fluorescence intensity of Nile red-loaded PF127-PAAIO gradually increases with the incubation time up to 6 h and fades away at 24 h of incubation. This result is expectable because folate-conjugated FA–PF127–PAAIO is taken up by KB cells via an FR-medicated endocytic pathway that can recycle the receptors back to the cell surface. Multiple rounds of internalization can be obtained by extending incubation to FA–PF127–PAAIO and this mechanism does not exist in the PF127–PAAIO system.

3.5. MRI Imaging of cells after MNPs internalization

The same preparations for the *in vitro* cellular uptake experiments were evaluated by MRI. This was done to evaluate the potential of FA–PF127–PAAIO as a targeted MR contrast agent to cancer cells that overexpress folate receptors. PF127–PAAIO was also measured for comparison. KB cells cultured with PF127–PAAIO or FA–PF127–PAAIO at various iron concentrations were incubated for 3 h. The T_2-weighted MR phantom images are shown in Fig. 10. The images of the cells incubated with FA–PF127–PAAIO show a significant negative contrast enhancement (signal darkening) over those cells incubated with PF127–PAAIO. The rapid and efficient folate receptor-mediated endocytosis leads to a distinguishable darkening of MR images of the cells incubated with FA–PF127–PAAIO as compared to PF127–PAAIO at the Fe concentration of 6 μg/mL. This result correlates to the MNPs concentration of 50 μg/mL determined by flow cytometry and CLSM studies. The enhancement of MR images of the cells after incubated with MNPs is defined by the following equation [18],

$$\text{Enhancement}\ (\%) = \frac{SI_{MNP} - SI_{Control}}{SI_{Control}} \times 100\% \quad (1)$$

where SI_{MNP} and $SI_{Control}$ are the signal intensities of MR images of the cells incubated with and without MNPs. At an iron concentration of 6 μg/mL, the MRI signal enhancement decreases from −10.37% for PF127–PAAIO to −29.75% for FA–PF127–PAAIO. The significant decrease in MRI intensity in PF127–PAAIO is observed at the MNP concentration as high as 30 μg/mL. Under these conditions the enhancement is −33.46%, while FA–PF127–PAAIO is −66.34%. Consistent with the MNP cellular uptake results obtained above, the T_2-weighted MR phantom images of FA–PF127–PAAIO, shown in Fig. 10, displays a profoundly increased negative contrast enhancement in comparison with the PF127–PAAIO without FA. Current clinical trials of four folate-linked drugs demonstrate that folate receptor-targeting holds great promise for increasing the potency while reducing toxicity of many cancer therapies [40]. Our results are also consistent with the remark that FA–PF127–PAAIO with the FA moiety shows a better cellular internalization into the FR overexpressing KB cells.

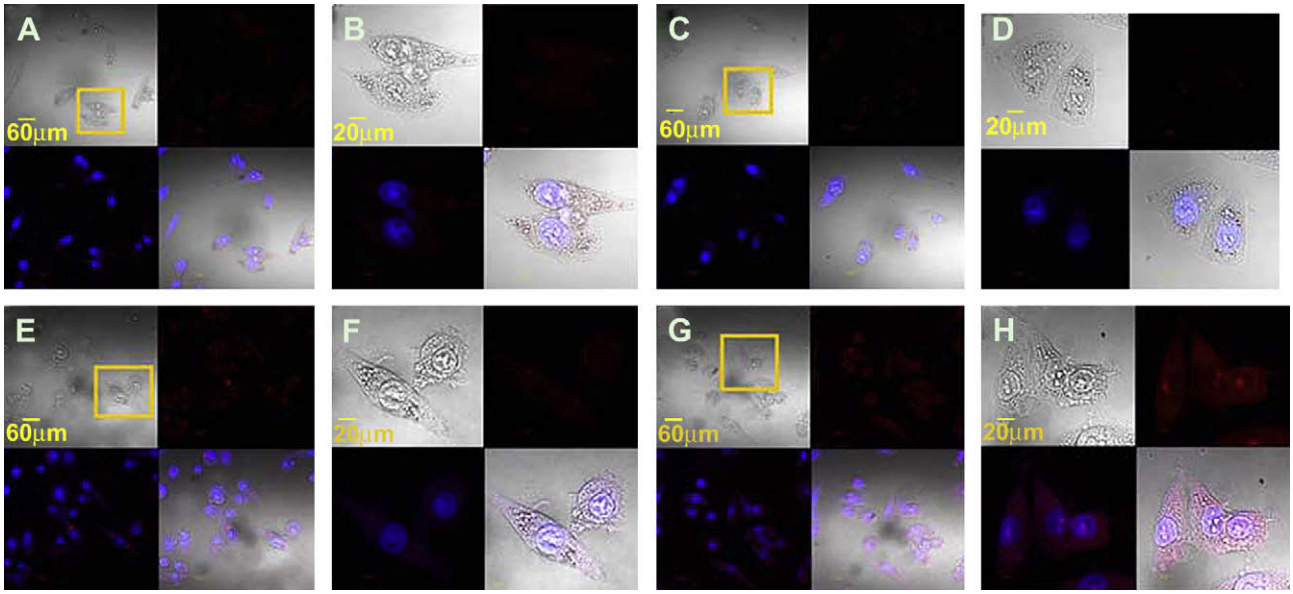

Fig. 8. Confocal microscopy analysis of PF127–PAAIO (A, B, E, F) and FA–PF127–PAAIO (C, D, G, H) at a concentration of 50 μg/ml internalized into KB cells after incubation with MNPs for 1 h (A–D) and 3 h (E–H).

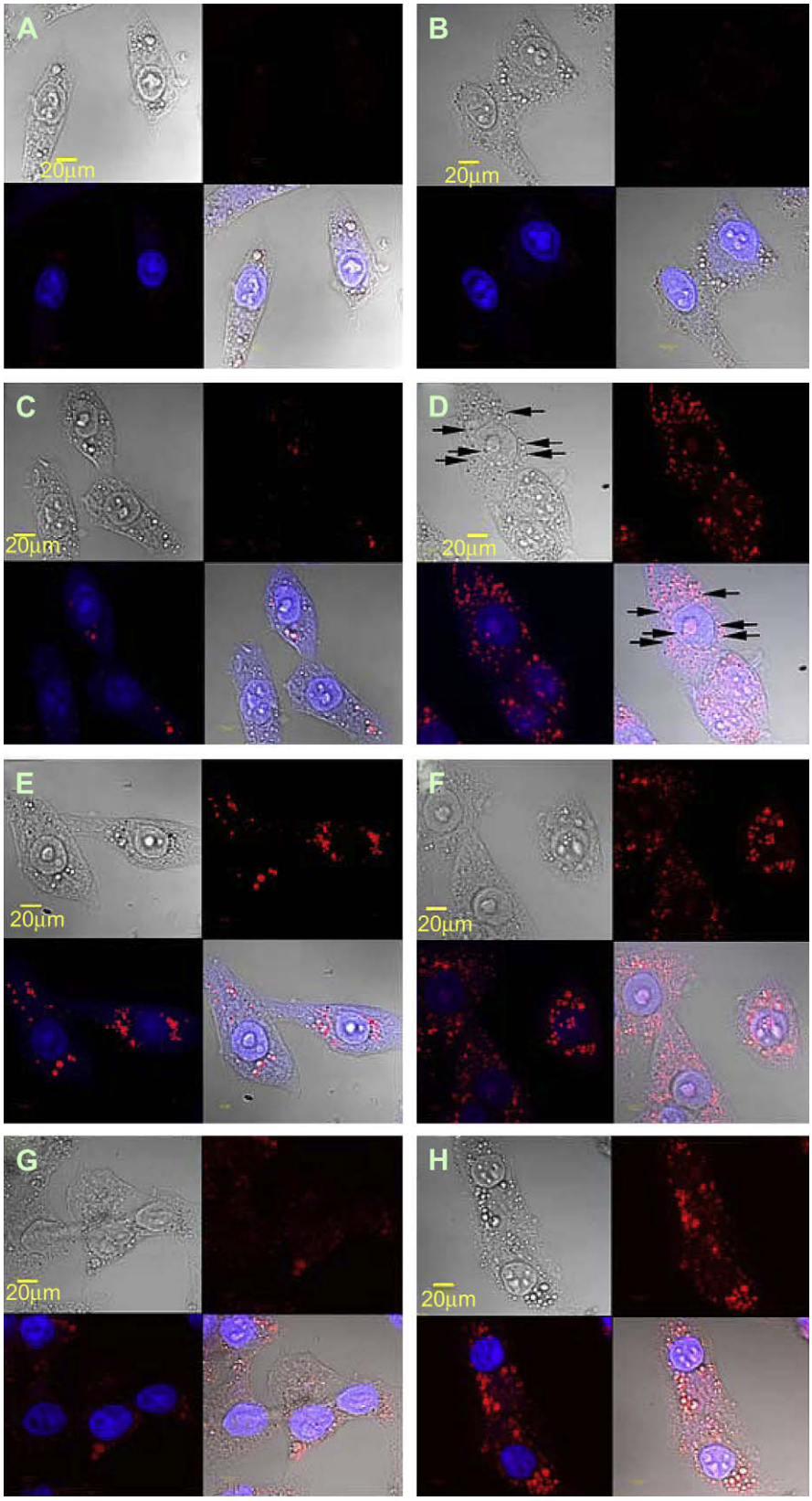

Fig. 9. Confocal microscopy analysis of PF127–PAAIO (A, C, E, G) and FA–PF127–PAAIO (B, D, F, H) at a concentration of 500 μg/ml internalized into KB cells after incubation with MNPs for 1 h (A, B), 3 h (C, D), 6 h (E, F), and 12 h (G, H).

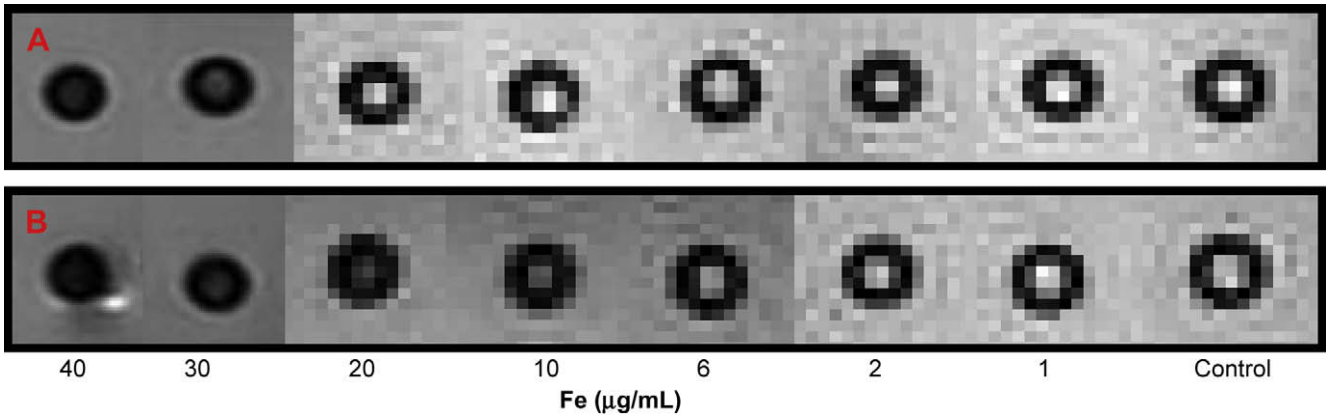

Fig. 10. T2-weighted MR phantom images of KB cells after incubation with the various concentrations of PF127–PAAIO (A) and FA–PF127–PAAIO (B) for 3 h.

4. Conclusions

In this study, PAA-bound Fe_3O_4 was synthesized by a one-pot reaction. PF127 and its derivative were grafted onto PAAIO by the chemical conjugation to yield the more stable and smaller MNP clusters which could be stored in lyophilized form and rapidly resuspended in DD water. The amount of polymer modified onto PAAIO was in the range of 60–70 wt%, revealing a higher efficiency of a MNP surface modification via a chemical reaction versus physical dispersion. The PF127-coated MNPs still retained high levels of superparamagnetic characteristics. The surface coating polymer on PAAIO was also the determining factor for the efficiency of cellular uptake. FA–PF127–PAAIO having the FA moiety showed a better cellular internalization in the FR overexpressing KB cells. The successful encapsulation of a fluorescent agent Nile red into PF127–PAAIO or FA–PF127–PAAIO illustrated the potential application for dual fluorescence and MR imaging. Furthermore, if Nile red was recognized as a hydrophobic drug, Nile red-loaded FA–PF127–PAAIO could be evaluated as a promising drug delivery carrier as well as a MRI contrast agent that specifically targets FR overexpressing tumor cells.

Acknowledgements

We are grateful for the financial support from the National Science Foundation of Taiwan under the grant number of NSC 95-2221-E037-006-MY3 and NSC 97-2320-B037-002. We also thank Dr. Yao Li Huang for the assistance in AAS measurements and Dr. James R. Carey for help in the preparation of this manuscript for publication.

Appendix

Figures with essential colour discrimination. Many of the figures in this article, especially Figures 8, 9 and 10, may be difficult to interpret in black and white. The full colour images can be found in the on-line version, at doi:10.1016/j.biomaterials.2009.06.004.

Appendix. Supporting information

Supplementary data associated with this article can be found in the online version, at doi:10.1016/j.biomaterials.2009.06.004.

References

[1] Osaka T, Matsunaga T, Nakanishi T, Arakaki A, Niwa D, Iida H. Synthesis of magnetic nanoparticles and their application to bioassays. Anal Bioanal Chem 2006;384:593–600.
[2] Gupta AK, Naregalkar RR, Vaidya VD, Gupta M. Recent advances on surface engineering of magnetic iron oxide nanoparticles and their biomedical applications. Nanomed 2007;2:23–39.
[3] Liang S, Wang Y, Yu J, Zhang C, Xia J, Yin D. Surface modified superparamagnetic iron oxide nanoparticles: as a new carrier for bio-magnetically targeted therapy. J Mater Sci 2007;18:2297–302.
[4] Sun C, Fang C, Stephen Z, Veiseh O, Hansen S, Lee D, et al. Tumor-targeted drug delivery and MRI contrast enhancement by chlorotoxin-conjugated iron oxide nanoparticles. Nanomed 2008;3:495–505.
[5] Yang Y, Jiang JS, Du B, Gan ZF, Qian M, Zhang P. Preparation and properties of a novel drug delivery system with both magnetic and biomolecular targeting. J Mater Sci 2009;20:301–7.
[6] Scarberry KE, Dickerson EB, McDonald JF, Zhang ZJ. Magnetic nanoparticle-peptide conjugates for in vitro and in vivo targeting and extraction of cancer cells. J Am Chem Soc 2008;130:10258–62.
[7] Lee HY, Li Z, Chen K, Hsu AR, Xu C, Xie J, et al. PET/MRI dual-modality tumor imaging using arginine–glycine–aspartic (RGD)-conjugated radiolabeled iron oxide nanoparticles. J Nucl Med 2008;49:1371–9.
[8] Zhang J, Rana S, Srivastava RS, Misra RD. On the chemical synthesis and drug delivery response of folate receptor-activated, polyethylene glycol-functionalized magnetite nanoparticles. Acta Biomater 2008;4:40–8.
[9] Sun C, Sze R, Zhang M. Folic acid–PEG conjugated superparamagnetic nanoparticles for targeted cellular uptake and detection by MRI. J Biomed Mater Res A 2006;78:550–7.
[10] Muthu MS, Singh S. Targeted nanomedicines: effective treatment modalities for cancer, AIDS and brain disorders. Nanomed 2009;4:105–18.
[11] Tosi G, Costantino L, Ruozi B, Forni F, Vandelli MA. Polymeric nanoparticles for the drug delivery to the central nervous system. Expert Opin Drug Deliv 2008;5:155–74.
[12] Peng XH, Qian X, Mao H, Wang AY, Chen ZG, Nie S, et al. Targeted magnetic iron oxide nanoparticles for tumor imaging and therapy. Int J Nanomedicine 2008;3:311–21.
[13] McCarthy JR, Weissleder R. Multifunctional magnetic nanoparticles for targeted imaging and therapy. Adv Drug Deliv Rev 2008;60:1241–51.
[14] Zhao HZ, Tan EC, Yung LY. Potential use of cholecalciferol polyethylene glycol succinate as a novel pharmaceutical additive. J Biomed Mater Res A 2008;84:954–64.
[15] Senthilkumar M, Mishra P, Jain NK. Long circulating PEGylated poly(D, L-lactide-co-glycolide) nanoparticulate delivery of docetaxel to solid tumors. J Drug Target 2008;16:424–35.
[16] Liu L, Guo K, Lu J, Venkatraman SS, Luo D, Ng KC, et al. Biologically active core/shell nanoparticles self-assembled from cholesterol-terminated PEG–TAT for drug delivery across the blood–brain barrier. Biomaterials 2008;29:1509–17.
[17] Zhang J, Misra RD. Magnetic drug-targeting carrier encapsulated with thermosensitive smart polymer: core-shell nanoparticle carrier and drug release response. Acta Biomater 2007;3:838–50.
[18] Chen TJ, Cheng TH, Chen CY, Hsu SC, Cheng TL, Liu GC, et al. Targeted herceptin–dextran iron oxide nanoparticles for noninvasive imaging of HER2/neu receptors using MRI. J Biol Inorg Chem 2009;14:253–60.
[19] Lee H, Yu MK, Park S, Moon S, Min JJ, Jeong YY, et al. Thermally cross-linked superparamagnetic iron oxide nanoparticles: synthesis and application as a dual imaging probe for cancer in vivo. J Am Chem Soc 2007;129:12739–45.
[20] Garinot M, Fievez V, Pourcelle V, Stoffelbach F, des Rieux A, Plapied L, et al. PEGylated PLGA-based nanoparticles targeting M cells for oral vaccination. J Control Release 2007;120:195–204.
[21] Jain TK, Morales MA, Sahoo SK, Leslie-Pelecky DL, Labhasetwar V. Iron oxide nanoparticles for sustained delivery of anticancer agents. Mol Pharm 2005;2:194–205.
[22] Liu TY, Hu SH, Liu KH, Shaiu RS, Liu DM, Chen SY. Instantaneous drug delivery of magnetic/thermally sensitive nanospheres by a high-frequency magnetic field. Langmuir 2008.
[23] Jain TK, Richey J, Strand M, Leslie-Pelecky DL, Flask CA, Labhasetwar V. Magnetic nanoparticles with dual functional properties: drug delivery and magnetic resonance imaging. Biomaterials 2008;29:4012–21.

[24] Gupta AK, Gupta M. Synthesis and surface engineering of iron oxide nanoparticles for biomedical applications. Biomaterials 2005;26:3995–4021.
[25] Butoescu N, Seemayer CA, Foti M, Jordan O, Doelker E. Dexamethasone-containing PLGA superparamagnetic microparticles as carriers for the local treatment of arthritis. Biomaterials 2009;30:1772–80.
[26] Butoescu N, Jordan O, Burdet P, Stadelmann P, Petri-Fink A, Hofmann H, et al. Dexamethasone-containing biodegradable superparamagnetic microparticles for intra-articular administration: physicochemical and magnetic properties, and in vitro and in vivo drug release. Eur J Pharm Biopharm 2009.
[27] Nasongkla N, Bey E, Ren J, Ai H, Khemtong C, Guthi JS, et al. Multifunctional polymeric micelles as cancer-targeted, MRI-ultrasensitive drug delivery systems. Nano Lett 2006;6:2427–30.
[28] Yang J, Lee CH, Ko HJ, Suh JS, Yoon HG, Lee K, et al. Multifunctional magneto-polymeric nanohybrids for targeted detection and synergistic therapeutic effects on breast cancer. Angew Chem Int Ed Engl 2007;46:8836–9.
[29] Hilgenbrink AR, Low PS. Folate receptor-mediated drug targeting: from therapeutics to diagnostics. J Pharm Sci 2005;94:2135–46.
[30] Yoo HS, Park TG. Folate-receptor-targeted delivery of doxorubicin nano-aggregates stabilized by doxorubicin–PEG–folate conjugate. J Control Release 2004;100:247–56.
[31] Sega EI, Low PS. Tumor detection using folate receptor-targeted imaging agents. Cancer Metastasis Rev 2008;27:655–64.
[32] Ge J, Hu Y, Biasini M, Dong C, Guo J, Beyermann WP, et al. One-step synthesis of highly water-soluble magnetite colloidal nanocrystals. Chemistry (Weinheim an der Bergstrasse, Germany) 2007;13:7153–61.
[33] Sachl R, Uchman M, Matejicek P, Prochazka K, Stepanek M, Spirkova M. Preparation and characterization of self-assembled nanoparticles formed by poly(ethylene oxide)-block-poly(epsilon-caprolactone) copolymers with long poly(epsilon-caprolactone) blocks in aqueous solutions. Langmuir 2007;23:3395–400.
[34] Mosmann T. Rapid colorimetric assay for cellular growth and survival: application to proliferation and cytotoxicity assays. J Immunol Methods 1983;65:55–63.
[35] Babic M, Horak D, Jendelova P, Glogarova K, Herynek V, Trchova M, et al. Poly(*N*, *N*-dimethylacrylamide)-coated maghemite nanoparticles for stem cell labeling. Bioconjug Chem 2009;20:283–94.
[36] Chen AL, Ni HC, Wang LF, Chen JS. Biodegradable amphiphilic copolymers based on poly(epsilon-caprolactone)-graft chondroitin sulfate as drug carriers. Biomacromolecules 2008;9:2447–57.
[37] Ma YH, Wu SY, Wu T, Chang YJ, Hua MY, Chen JP. Magnetically targeted thrombolysis with recombinant tissue plasminogen activator bound to polyacrylic acid-coated nanoparticles. Biomaterials 2009.
[38] Chen S, Li Y, Guo C, Wang J, Ma J, Liang X, et al. Temperature-responsive magnetite/PEO–PPO–PEO block copolymer nanoparticles for controlled drug targeting delivery. Langmuir 2007;23:12669–76.
[39] Kamen BA, Capdevila A. Receptor-mediated folate accumulation is regulated by the cellular folate content. Proc Natl Acad Sci USA 1986;83:5983–7.
[40] Low PS, Henne WA, Doorneweerd DD. Discovery and development of folic-acid-based receptor targeting for imaging and therapy of cancer and inflammatory diseases. Acc Chem Res 2008;41:120–9.